Atomic-scale magnetic dissipation from spin-dependent adhesion hysteresis

E. Y. Vedmedenko,* Q. Zhu, U. Kaiser, A. Schwarz, and R. Wiesendanger

Institute of Applied Physics and Microstructure Research Center, University of Hamburg, Jungiusstraße 11, 20355 Hamburg, Germany

(Received 29 September 2011; revised manuscript received 30 January 2012; published 8 May 2012)

In this paper we develop a realistic theoretical understanding of the atomic-scale spin-dependent dissipation observed in recent magnetic exchange force microscopy experiments. The origin of dissipation is investigated using Monte Carlo energy minimization techniques for experiments performed with an Fe-coated tip on the antiferromagnetic insulator NiO(001). Our calculations demonstrate that adhesion hysteresis is site as well as distance dependent. The magnitude of the computed spin-dependent adhesion hysteresis agrees well with the experimentally measured magnetic dissipation. Particularly, we show that this mechanism does not necessarily involve spin flips but includes the previously proposed Caldeira-Leggett-type dissipation as a special case.

DOI: 10.1103/PhysRevB.85.174410 PACS number(s): 75.70.Rf, 68.37.Ps, 68.47.Gh, 75.47.Lx

I. INTRODUCTION

Spin-sensitive studies of magnetic surfaces at the atomic scale are currently a very active field of research. Most experiments visualizing magnetic surface structures with atomic resolution were performed by employing spin-polarized scanning tunneling microscopy (SP-STM).[1] Recently, magnetic exchange force microscopy (MExFM) experiments demonstrated that spin mapping with atomic resolution can also be achieved with an atomic force microscopy (AFM) based setup,[2–4] thereby enabling the investigation of magnetic insulators.[2] Additionally, the dynamic mode of operation used to acquire MExFM data allows to simultaneously measure the dissipated energy due to nonconservative tip-sample interactions as reported in Refs. 1,4 without theoretical analysis. The dissipative signal in MExFM is to some extent analogous (and at the same time complementary) to inelastic tunneling processes of magnetic origin. Recently, the latter gave important new insights into atomic-scale magnetism on conductive samples.[5,6] However, insulators such as NiO can only be studied with MExFM.

While possible atomic-scale dissipative mechanisms for nonmagnetic tip-sample systems have been discussed intensively in the literature (see Ref. 7 for a review), we are aware of only two publications addressing atomic-scale magnetic dissipation, i.e., spin excitations via friction following Landau-Lifshitz-Gilbert dynamics[8] and spin-phonon coupling within the Caldeira-Leggett model.[9] Spin excitation is a straightforward mechanism for a dissipation signal of magnetic origin. However, this mechanism is not very efficient due to the large mismatch between the oscillation frequency of the cantilever in the dynamic mode (≈158 kHz in our case) and typical spin excitation resonances (GHz regime). Note that analogously, phonon excitations cannot be responsible for the experimentally observed magnitude of the dissipation contrast found between chemically different species in atomically resolved AFM images.[10] Instead, the site-dependent adhesion hysteresis appeared to be the dominating mechanism for nonmagnetic dissipation.[7] Due to the adhesion hysteresis strong chemical interactions at small tip-sample distances lead to reversible but hysteretic reconfigurations of atoms during approach and retraction of each oscillation cycle.[11]

Here, we analyze magnetic dissipation data obtained with an Fe-coated tip on the antiferromagnetic insulator NiO(001) and provide simulations using Monte Carlo minimization techniques. We demonstrate that the magnetic dissipation is complementary to the *normal* nonmagnetic adhesion hysteresis: For a magnetic tip-sample system the magnetic exchange interaction contributes to the total interaction. As a result, the hysteretic reconfiguration at the tip apex, and hence the energy dissipation involved in this process, depends on the relative orientation between the interacting spins, which in turn lead to a *spin-dependent* dissipation. Based on our calculations we are able to explain the experimentally observed dissipation contrast on chemically equivalent Ni and on O surface atoms by spin-dependent adhesion hysteresis.

II. DISSIPATION MEASUREMENT

To understand the origin of the dissipation signal, we shortly introduce the way of data acquisition: MExFM combines the atomic-resolution capabilities of AFM with spin sensitivity by using a magnetic tip mounted on the free end of a cantilever as a probe.[12] For detection the frequency modulation (FM) scheme is employed, where the cantilever self-oscillates with constant amplitude A_0 at its resonance frequency f_0.[13] In the presence of tip-sample interactions, f_0 of the free cantilever is shifted by Δf. To measure at a constant tip-sample interaction, Δf is kept constant by adjusting z accordingly during scanning via a feedback loop. The resulting $z(x,y)$ image is the topography. On the atomic scale z corrugations reflect the relative strengths of the electron-mediated short-range interactions, i.e., the chemical interaction and for magnetic tip-sample systems the magnetic exchange interaction as well. Simultaneously, A_0 is kept constant by adjusting the excitation amplitude a_{exc} with a second feedback loop that drives the cantilever oscillation. The applied excitation amplitude a_{exc} compensates for the dissipated energy E_{D} due to nonconservative tip-sample interactions.[14] Thus, $a_{\mathrm{exc}}(x,y)$ and $E_{\mathrm{D}}(x,y)$ are called the dissipation image. Note that the amount of energy dissipated per oscillation cycle can be easily calculated using[15]

$$\Delta E_{\mathrm{D}} = \frac{\pi c_z A_0^2}{Q}\left(\frac{a_{\mathrm{exc}}}{a_{\mathrm{exc},0}} - 1\right), \tag{1}$$

where c_z is the spring constant of the cantilever, $a_{\mathrm{exc},0}$ is the excitation amplitude required to compensate intrinsic losses

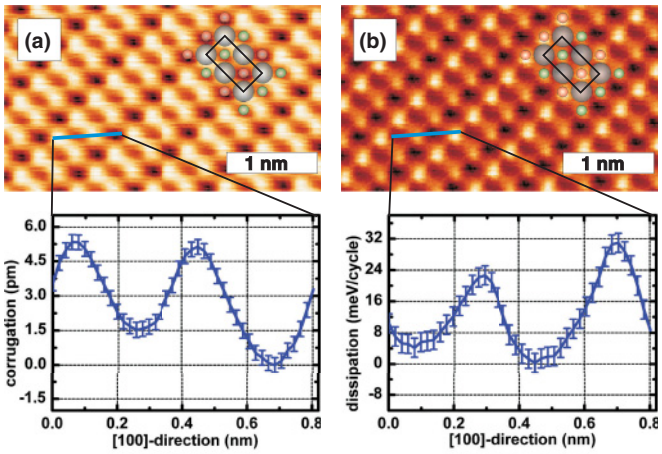

FIG. 1. (Color online) Atomically resolved MExFM topography image (a) and simultaneously recorded dissipation image (b). Displayed are the unit cell averaged data (Ref. 17). The ball model shows the chemical and magnetic structure of the surface. Line sections along the [100] direction of the unit cell visualize the magnitude of the spin-dependent contrast due to conservative (a) and nonconservative (b) tip-sample interactions, respectively. Note that the images were obtained in the attractive noncontact regime ($\Delta f = -23.4$ Hz) and that $A_0 = 6.65$ nm is large compared to the characteristic decay length of the short-ranged interactions that dominate contrast formation on the atomic scale.

determined far away form the surface, and Q is the quality factor of the resonant oscillation.

Figure 1 displays atomically resolved spin-dependent unit cell averaged experimental data obtained with an Fe tip on NiO(001) as presented by us previously.[1,2] The spin-carrying d electrons localized at the Ni atoms are coupled ferromagnetically along the ⟨110⟩ directions and antiferromagnetically between {111} planes by superexchange via the O atoms. Hence, a row-wise antiferromagnetic order emerges at the (001) surface. The topography image (a) obtained with an Fe-coated tip reproduces the chemical arrangement of atoms at the (001) surface due to the presence of chemical interactions as well as the row-wise antiferromagnetic order due to the presence of the magnetic exchange interaction. Since anions on ionic surfaces generally interact more strongly with metal tips than cations,[16] O sites are imaged as maxima and Ni sites as minima. This assignment is consistent with the row-wise magnetic contrast visible on minima, which reflect the spin-carrying Ni cations. The ball model depicts the positions of the O (gray) and Ni sites (red and green to indicate opposite spin orientations). The simultaneously recorded dissipation image (b) also exhibits a row-wise contrast on Ni atoms with opposite spin orientation. Peculiarly, there seems to be an additional but weaker contrast between rows of O atoms with Ni atoms of opposite spin orientations in the layer below, which is absent in the topography signal.

The line sections in (c) and (d) along the [110] direction visualize the magnitudes of the site- and spin-dependent topography and dissipation signals, respectively. The spin-dependent contrast between Ni atoms with opposite spin orientations is about 1.5 pm and thus much smaller than the chemical contrast between Ni and O atoms. No difference is visible between O atoms. In the dissipation signal the contrast is inverted; i.e., more energy is dissipated above the Ni atoms than above the O atoms. The magnetic dissipation on Ni atoms, i.e., the energy difference between Ni atoms with opposite spin orientations, is about 13.3 meV/cycle. For O atoms with oppositely oriented spins at the Ni atoms below them the magnetic dissipation is about 6.2 meV/cycle.

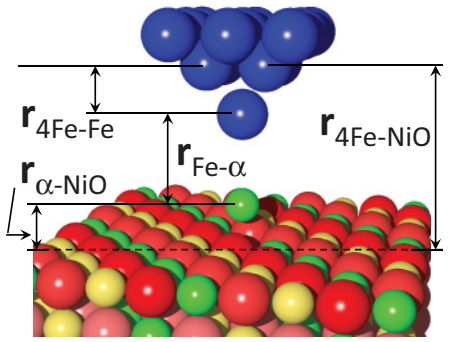

FIG. 2. (Color online) Tip-sample geometry and definition of distances used in the simulations. Green and yellow balls denote "up" and "down" Ni atoms, respectively, while red balls correspond to the oxygen atoms. α indicates the four different positions on the surface atoms Ni↑, Ni↓, O↑, and O↓. The tip-sample distance is defined as $r_{4\mathrm{Fe-NiO}}$. The distances $r_{\mathrm{Fe}-\alpha}$, $r_{\alpha-\mathrm{NiO}}$, and $r_{4\mathrm{Fe}-\mathrm{Fe}}$ correspond to the distances between the foremost Fe atom and the studied atom, the studied atom and the unperturbed surface, and the studied atom and the rest of the tip, respectively.

III. THEORETICAL MODEL

To investigate the origin of the large spin-dependent dissipation on Ni and O surface sites, we model the coupled tip-sample systems including all magnetic and nonmagnetic interactions between tip and sample on an atomistic level.

A. Geometry

The geometry of the system under investigation is defined in Fig. 2. As a model for the Fe tip we used a pyramidal 14-atom cluster of bcc(001) stacking with parameters taken from Ref. 34. For the sake of simplicity only vertical equilibrium motions of the tip with $\partial r/\partial t \to 0$ have been permitted. The tip-sample distance $r_{4\mathrm{Fe}-\mathrm{NiO}}$ has been defined as the distance between the second layer of the pyramidal cluster consisting of four Fe atoms and the unperturbed surface of NiO. The foremost Fe atom of the tip was free to relax. The rocksalt structure of the NiO crystal has been represented by a slab with dimensions $8 \times 8 \times 8$ interatomic distances a. According to the theoretical[18] as well as experimental studies[19–21] the relaxation of a bulk-terminated, clean NiO(001) surface layer is smaller than 3% of an ideal interlayer distance while the relaxation of deeper layers is negligible. Therefore, we assume a bulk-terminated NiO(001) structure without rhombohedral distortion with vertical structural relaxation of the surface atomic layer only. Below its Néel temperature of 525 K, NiO is a collinear antiferromagnet with ferromagnetic {111} sheets stacked in an antiferromagnetic order. The two oppositely magnetized sorts of Ni atoms ({111} planes) are presented

as green and yellow balls in Fig. 2. The red balls represent the oxygen atoms. The tip-sample distance $r_{4\mathrm{Fe}-\mathrm{NiO}}$ has been defined as the distance between the second layer of the Fe tip consisting of four Fe atoms and an unperturbed surface layer of NiO. The distances between the foremost Fe atom and the studied atom $r_{\mathrm{Fe}-\alpha}$, the studied atom and the unperturbed surface $r_{\alpha-\mathrm{NiO}}$, and the studied atom and the rest of the tip $r_{4\mathrm{Fe}-\alpha}$ have been analyzed as a function of the tip-sample distance. The studied atom α is either Ni↑, Ni↓, O↑, or O↓, where the arrows at the O atoms refer to the spin orientations of the Ni atoms in the layer underneath.

B. Simulation procedure

All structural relaxations have been performed in the framework of the standard Monte Carlo (MC) technique[22,23] or by steepest-descent energy minimization including generalized Buckingham potentials and magnetic exchange. Since the employed model allows for movements along the vertical axis only, these two methods give identical results at zero temperature.[24] The Hamiltonian of the coupled tip-sample system can be expressed by

$$\mathcal{H} = \sum_{i<j} V_{ij}(r) + J_{ij}(r) \sum_{i<j} \vec{S}_i \vec{S}_j, \tag{2}$$

where the summation includes all considered interatomic interactions with the corresponding distance-dependent potential $V(r)$ and the exchange parameter $J(r)$. In the simulations all interactions within the NiO slab and the Fe tip as well as between all tip and sample atoms were considered. The coefficients in Eq. (2) have been taken from *ab initio* calculations or experiments.[25] No parameters were fitted to match the experimental data.

First, the NiO crystal has been relaxed without the Fe tip. The relaxed NiO surface showed an outward expansion of Ni and inward contraction of O atoms (rumpling). This result is in good agreement with molecular dynamics calculations[26] and experiments.[21] For the calculations including the magnetic tip we considered an unperturbed initial configuration of the Fe tip. However, the foremost tip atoms were able to relax during the simulation. A starting distance $r_{4\mathrm{Fe}-\mathrm{NiO}} = 6.2$ Å was chosen to ensure an initially well-separated tip-sample system. In the next step $r_{4\mathrm{Fe}-\mathrm{NiO}}$ was decreased stepwise. For each tip position the system was relaxed during n_0 initial steps plus N additional MC steps until convergence was reached. At each MC step the positions of the foremost Fe atom as well as of each of the 24 surface atoms have been sampled within a step width of $k = \pm 10^{-2} \ldots 10^{-4}$ Å and accepted or rejected according to the Metropolis probability or the steepest-descent procedure. Note that during the relaxation, interactions between all NiO and Fe atoms have been considered. The condition for the convergency was set as $|r_{\mathrm{Ni}}(n_0 + N) - r_{\mathrm{Ni}}(n_0)| < k$ and $|r_{\mathrm{Fe}}(n_0 + N) - r_{\mathrm{Fe}}(n_0)| < k$. The coarser resolution was applied only in cases when comparable calculations with $k = \pm 10^{-4}$ Å provided similar results. For the sake of simplicity we did not allow for spin flips in this set of simulations; i.e., the magnetization of Fe atoms was always "upward."

C. Atomic and magnetic potentials

The effective chemical potential for atomistic simulations on NiO includes pairwise ionic as well as Buckingham-type potentials of general form[25]

$$V_{\mathrm{NiO}} = \frac{q_i q_j}{r} + A\, e^{-r/\rho} - \frac{C}{r^6}, \tag{3}$$

with ρ extension of the occupied spin orbitals, q ionic charges, and parameters A and C. The parameter set for NiO is by no means unique. The coefficients A and C have been generated variationally to best fit experimental data for bulk NiO.[25] While the electrical charges can be considered as localized in the bulk of this ceramic material they become more and more delocalized near the surface of the crystal. The values of the effective Mulliken charges vary in the literature from $0.99e$[27] to $1.5e$.[28] To adopt the simplest, most obvious parametrization consistent with experimental data we used nominal ionic charges Ni^{2+} and O^{2-} for the bulk part of the crystal, while varying q_{eff} between $0.99e$ and $1.5e$ for the surface layer. Stable structures have been obtained in the range of $q_{\mathrm{eff}} = 1.25e \ldots 1.35e$. In the following we use data for $q_{\mathrm{eff}} = 1.3e$ for the surface layer. In our computations, the interaction cutoff length is taken as $r_{\mathrm{co}} \simeq 6a$. This corresponds to ≈520 bonds in NiO.

Magnetic structure of NiO originating from the Anderson-type superexchange is of the antiferromagnetic AFII order, characterized by planes of opposite magnetization which are stacked in the [111] direction. The superexchange interactions in NiO are long ranged and have a ferromagnetic character within the (111) planes between nearest-neighboring Ni spins and antiferromagnetic character between the (111) planes, i.e., next-nearest-neighboring Ni spins. The superexchange interactions in NiO have been recently mapped onto the Heisenberg Hamiltonian.[29] In Ref. 29 the ferromagnetic $[J_1(r) > 0]$ and antiferromagnetic $[J_2(r) < 0]$ exchange parameters have been calculated as a function of the lattice constant which might change under deformation. We have fitted these data by an RKKY-like expression

$$J_k(r) = \frac{c\, e^{-k_2 r} \sin(k_1 r + b)}{r^3}, \tag{4}$$

where k_1 and k_2 correspond to the Fermi wave vectors of majority and minority states, while c and b are parameters. The best fit for $J_1(r)$ has been obtained with $c = 30.85$ meV/Å^3, $b = 10.87$, $k_1 = -3.0720$ Å^{-1}, and $k_2 = 0.68410$ Å^{-1}, while for $J_2(r)$ with $a = -7390$ meV/Å^3, $b = 9.139$, $k_1 = -0.05006$ Å^{-1}, and $k_2 = 0.00269$Å^{-1}. A similar scheme has been used for calculations of the iron tip. The effective Morse potential reads

$$V_{\mathrm{Fe}} = D[e^{-2\alpha(r-r_0)} - 2e^{-\alpha(r-r_0)}] \tag{5}$$

with $D = 0.4174$ eV, $r_0 = 2.845$ Å, and $\alpha = 1.3885$ Å^{-1} being experimentally determined parameters.[30] The ferromagnetic exchange interaction $J_{\mathrm{Fe}}(r)$ calculated in Ref. 31 has been fitted by Eq. (4) with $a = -0.4132$ meV/Å^3, $b = 1.355$, $k_1 = 1.284$ Å^{-1}, and $k_2 = 0.1513$Å^{-1}.

To minimize the tip-sample interaction energy we have adapted the data of first-principles calculations.[32] The total force curves from Ref. 32 have been integrated to obtain

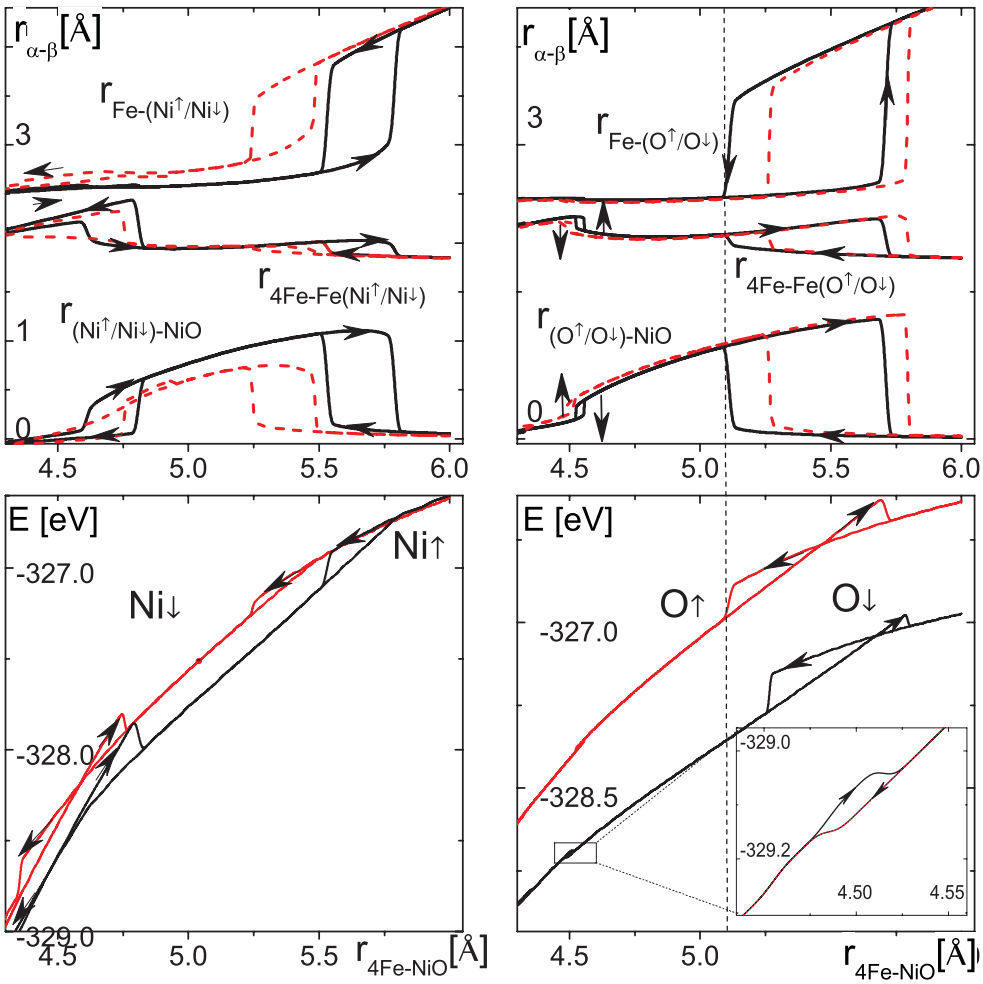

FIG. 3. (Color online) Calculated equilibrium interatomic distances (upper panels) and total energy E_t (lower panels) above Ni atoms (left) and O atoms (right) as a function of the tip-sample distance $r_{4Fe-NiO}$. The used notations are indicated in the inset in the lower left panel. Solid (black) and dashed (red) lines correspond to "spin up" (parallel) and "spin down" (antiparallel) orientations with respect to the Fe tip atom. All curves in the upper panels exhibit hysteresis (arrows indicate approach and retrace cycles), which result in the site- and spin-dependent energy dissipation visible in the lower panels.

the distance-dependent potentials, and recursively separated to obtain the pairwise interactions between the apex Fe atom of the tip with its surface counterparts. These potentials include all chemical as well as magnetic contributions and are of the form[32]

$$V(r_{Fe-\alpha}) = -r_{Fe-\alpha}\left(\frac{r_{Fe-\alpha}}{d}\right)^{-2n}\left(\frac{A}{1-2n} - \frac{B(r_{Fe-\alpha}/d)^n}{1-n}\right) \quad (6)$$

with α corresponding to Ni↑, Ni↓, O↑, or O↓, and fitting parameters A, B, n. The potential $V(r_{Fe-\alpha})$ describes ≈340 bonds between all considered Fe and NiO atoms.

IV. RESULTS AND DISCUSSION

Our calculations show that due to the mutual interaction between tip and sample atoms the potential landscapes of the interacting atoms exhibit more than one minima. At certain distances the energy barrier between two minima vanished and the atom jumped abruptly toward its new position. This can directly be seen in the distance-dependent equilibrium interatomic separations at zero temperature plotted in the upper panel of Fig. 3. On all sites the foremost Fe tip atom as well as the surface atom directly underneath exhibits the above-mentioned abrupt positional changes. The distances at which these jumps occur are site and spin dependent. Moreover, they are hysteretic, i.e., different during approach and retrace cycles.

To quantify the dissipated energy due to the observed hysteresis we have calculated the total energy of the system E_t for all four different sites on NiO(001), including all magnetic and nonmagnetic contributions for all considered bonds, as a function of $r_{4Fe-NiO}$ (see lower panel of Fig. 3). At several $r_{4Fe-NiO}$ values, jumps in atomic distances appear and E_t abruptly decreases; i.e., energy is released. Therefore, the energy curves are also hysteretic and exhibit a distinctive distance dependence.

The sum of all jumps for a given atom in Fig. 3 is the total energy dissipated during one oscillation cycle over a certain distance regime (ΔE_t). These calculated values can directly

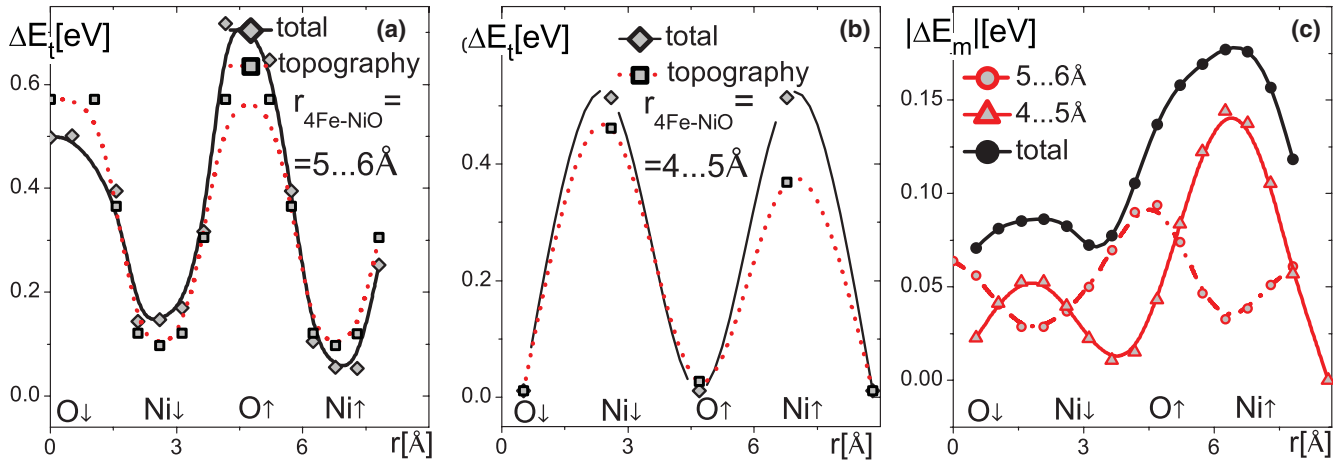

FIG. 4. (Color online) Total and nonmagnetic energy along the [001] direction of NiO(001) for $r_{4\text{Fe}-\text{NiO}} = 5...6$ Å (a) and $r_{4\text{Fe}-\text{NiO}} = 4...5$ Å (b). In (c) the difference between total and nonmagnetic contribution, i.e., the magnetic dissipation, is shown for $r_{4\text{Fe}-\text{NiO}} = 5...6$ Å (triangles) and $r_{4\text{Fe}-\text{NiO}} = 4...5$ Å (hollow circles). Additionally, the sum of both curves is plotted (black solid circles).

be compared with the experimentally determined values. ΔE_t is equivalent to the area enclosed by the corresponding force curve $-\partial E(r_{4\text{Fe}-\text{NiO}})/\partial r_{4\text{Fe}-\text{NiO}}$, which is typically regarded as a measure for the energy dissipation. Note that for our highly symmetric tip multiple distinct hysteresis loops are present in all curves of Fig. 3. More realistic complex tip geometries could probably result in a continuous distance dependence.

In Fig. 4 the site dependence along the [001] direction of the total and the nonmagnetic part of the dissipated energy is displayed for two distance regimes, i.e., $r_{4\text{Fe}-\text{NiO}} = 5...6$ Å (a) and $r_{4\text{Fe}-\text{NiO}} = 4...5$ Å (b), respectively. Each point corresponds to the sum of all jumps shown in Fig. 3 in the respective distance regime. For $r_{4\text{Fe}-\text{NiO}} < 4.3$ Å the Fe tip becomes unstable at some lateral positions between Ni and O surface atoms in our calculations. Therefore, the curves in Fig. 4(b) are spline approximations of data obtained directly above Ni and O atoms. Interestingly, the site of largest dissipation depends on $r_{4\text{Fe}-\text{NiO}}$. This is already evident in Fig. 3, where jumps in energy for Ni atoms are larger than those for O atoms at $r_{4\text{Fe}-\text{NiO}} = 4...5$ Å, while the opposite is true at $r_{4\text{Fe}-\text{NiO}} = 5...6$ Å. Furthermore, magnitude and sign of the dissipated energy depends on the distance regime, through which the tip oscillates. To obtain the spin-dependent dissipation, the nonmagnetic contribution is subtracted from the total dissipation; cf. (c). For $A_0 = 1$ Å the contrast is inverted, if the distance regime is changed from $r_{4\text{Fe}-\text{NiO}} = 5...6$ Å to $r_{4\text{Fe}-\text{NiO}} = 4...5$ Å. Thus, for small amplitudes the experimentally observed contrast depends also on A_0. Note that such small amplitudes are experimentally accessible and actually often used nowadays in tuning fork q-plus setups (see Ref. 33). Since the experimental data presented in Fig. 1 are recorded with $A_0 = 6.65$ nm, the sum of both distance regimes, i.e., the black curve in (c), is displayed as well. The range of about 100 meV between minimum and maximum is close to the experimental value. Note that for distances larger than 6 Å no further jumps occur. Therefore, for sufficiently large amplitudes the contrast only depends on the tip-sample distance at the lower turnaround point, but becomes independent of A_0.

As for the experimental data, the calculated dissipated energy ΔE_t in all three curves of Fig. 4(c) is different on the four chemically and magnetically distinctive sites, i.e., Ni↑, Ni↓, O↑, and O↓, and occurs at interstitial sites as well. Moreover, the sign of the contrast in Fig. 1(d) coincides with the calculated contrast for the sum. Considering that the atomic configurations of model tip and real tip are probably quite different, the order of magnitude (tens of meV) for the calculated spin-dependent dissipation contrast is in reasonably good agreement with the experimental data.

V. CONCLUSION

In conclusion, energy minimization of the NiO(001)/Fe-tip system shows a strikingly complex hysteretic site-, distance-, and spin-dependent behavior at tip-sample separations typically occurring in MExFM measurements. Since the energy curves are different during approach and retrace of each oscillation cycle, energy is dissipated. Since the magnitude of the calculated dissipation due to spin-dependent adhesion hysteresis agrees qualitatively well with the experimentally observed values, we conclude that this mechanism can dominate the phenomenon of magnetic dissipation. Moreover, since we did not allow for spin flips in our model, such spin flips are not a prerequisite for magnetic dissipative contrast as proposed in the Caldeira-Leggett model.[9] However, the released energy may subsequently excite versatile spin flips either in the tip or in the sample.

ACKNOWLEDGMENTS

Support by the DFG (SFB 668, projects A11 and A5) and by the Cluster of Excellence "Nanospintronics" Hamburg is gratefully acknowledged. E.Y.V. acknowledges discussions with A. Ernst.

*vedmeden@physnet.uni-hamburg.de

[1]R. Wiesendanger, Rev. Mod. Phys. **81**, 1495 (2009).
[2]U. Kaiser, A. Schwarz, and R. Wiesendanger, Nature (London) **446**, 522 (2007).
[3]R. Schmidt, C. Lazo, H. Hölscher, U. H. Pi, V. Caciuc, A. Schwarz, R. Wiesendanger, and S. Heinze, Nano Lett. **9**, 200 (2009).
[4]R. Schmidt, C. Lazo, U. Kaiser, A. Schwarz, S. Heinze, and R. Wiesendanger, Phys. Rev. Lett. **106**, 257202 (2011).
[5]S. Loth, M. Etzkorn, C. P. Lutz, D. M. Eigler, and A. J. Heinrich, Science **329**, 1628 (2010).
[6]A. A. Khajetoorians, B. Chilian, J. Wiebe, S. Schuwalow, F. Lechermann, and R. Wiesendanger, Nature (London) **467**, 1084 (2010).
[7]S. Morita, R. Wiesendanger, and E. Meyer, eds., *Noncontact Atomic Force Microscopy* (Springer Verlag, Berlin-Heidelberg, 2002).
[8]M. P. Magiera, L. Brendel, D. E. Wolf, and U. Nowak, Europhys. Lett. **87**, 26002 (2009).
[9]F. Pellegrini, G. E. Santoro, and E. Tosatti, Phys. Rev. Lett. **105**, 146103 (2010).
[10]M. Gauthier and M. Tsukada, Phys. Rev. B **60**, 11716 (1999).
[11]N. Sasaki and M. Tsukada, Jpn. J. Appl. Phys. **39**, L1334 (2000).
[12]A. Schwarz and R. Wiesendanger, Nano Today **3**, 28 (2008).
[13]T. R. Albrecht, P. Grütter, D. Horne, and D. Rugar, J. Appl. Phys. **69**, 668 (1991).
[14]H. Hölscher, B. Gotsmann, W. Allers, U. D. Schwarz, H. Fuchs, and R. Wiesendanger, Phys. Rev. B **64**, 075402 (2001).
[15]B. Anczykowski, B. Gotsmann, H. Fuchs, J. P. Cleveland, and V. B. Ellings, Appl. Surf. Sci. B **140**, 376 (1999).
[16]G. Teobaldi, K. Lammle, T. Trevethan, M. Watkins, A. Schwarz, R. Wiesendanger, and A. L. Shluger, Phys. Rev. Lett. **106**, 216102 (2011).
[17]All unit cells in the raw data are averaged to obtain a single averaged unit cell, which is tiled to a unit cell averaged image with a better signal-to-noise-ratio. Error bars in the line sections indicate the standard deviation calculated after the averaging procedure.
[18]H. Momida and T. Oguchi, J. Phys. Soc. Jpn. **72**, 588 (2003).
[19]C. G. Kinniburgh and J. A. Walker, Surf. Sci. **63**, 274 (1977).
[20]M. R. Welton-Cook and M. Prutton, J. Phys. C **13**, 3993 (1980).
[21]T. Okazawa, Y. Nakagawa, and Y. Kido, Phys. Rev. B **69**, 125412 (2004).
[22]E. E. Zhurkin and M. Hou, J. Phys.: Condens. Matter **12**, 6735 (2000).
[23]A. A. Dzhurakhalov and M. Hou, Phys. Rev. B **76**, 045429 (2007).
[24]M. C. Payne, M. P. Teter, D. C. Allan, T. A. Arias, and J. D. Joannopoulos, Rev. Mod. Phys. **64**, 1045 (1992).
[25]C. X. Guo, O. Warschkow, D. E. Ellis, V. P. Dravid, and E. C. Dickey, J. Am. Ceram. Soc. **84**, 2677 (2001).
[26]T. E. Karakasidis, D. G. Papageorgius, and G. A. Evangelakis, Appl. Surf. Sci. **162–163**, 223 (2000).
[27]A. M. Ferrari, C. Pisani, F. Cinquini, L. Giordano, and G. Pacchioni, J. Chem. Phys. **127**, 174711 (2007).
[28]T. Bredow and A. R. Gerson, Phys. Rev. B **61**, 5194 (2000).
[29]G. Fischer, M. Dane, A. Ernst, P. Bruno, M. Lueders, Z. Szotek, W. Temmerman, and W. Hergert, Phys. Rev. B **80**, 014408 (2009).
[30]L. A. Girifalco and V. G. Weizer, Phys. Rev. **114**, 687 (1959).
[31]I. Turek, V. Drchal, J. Pajda, J. Kudrnovsky, and P. Bruno, Phys. Rev. B **64**, 174402 (2001).
[32]H. Momida and T. Uguchi, Surf. Sci. **590**, 42 (2005).
[33]F. J. Giessibl, Rev. Mod. Phys. **75**, 1287 (2003).
[34]C. Lazo, V. Caciuc, H. Hölscher, and S. Heinze, Phys. Rev. B **78**, 214416 (2008).